

Article

Stabilize and Flatten Multi-Wavelength Erbium-Doped Fiber Laser through Accurate Hybrid Dual-Ring-Configuration Control

Xudong Zhang ¹, Tieying Li ¹ and Jiuru Yang ^{2,*} 

¹ College of Electric Engineering, Heilongjiang University, Harbin 150080, China; 2161304@s.hlju.edu.cn (X.Z.); 2171233@s.hlju.edu.cn (T.L.)

² Key Lab of Electronics Engineering, College of Heilongjiang Province, Heilongjiang University, Harbin 150080, China

* Correspondence: yangjr@hlju.edu.cn; Tel.: +86-451-8660-8504

Received: 20 October 2017; Accepted: 8 December 2017; Published: 12 December 2017

Abstract: In order to enhance the practicality of multi-wavelength erbium-doped fiber lasers (MWEDFLs), a novel hybrid dual-ring configuration is proposed in this article, which can flatten the outputs through an optical nonlinear-polarization-rotation-based ring cavity and stabilize the shifts of power and central wavelength of oscillations through an electrical fuzzy-control-based feedback. The experiment results show that, our scheme achieves more than 10 stable oscillations with the dramatic improvements in flatness and working stability. Under dual-ring configuration, the output intensity of MWEDFL reaches ~ -7.5 dBm with the flatness of ± 0.42 dB. And the in-stabilities in terms of power and central wavelength are respectively constrained ± 0.182 dBm and ± 0.029 nm within 10-h continuous operation.

Keywords: multi-wavelength erbium-doped fiber laser; nonlinear polarization rotation; hybrid control; working stability; flatness

1. Introduction

Owing to high efficiency of erbium-doped fiber (EDF), multi-wavelength erbium-doped fiber lasers (MWEDFLs) have become one of hot topics in optical fiber communication, sensing and testing systems since the 1990s [1–4]. The first comb-filter-based MWEDFLs is reported by Chow which operates at ultralow temperature (-77 K, liquid nitrogen) [5]. To overcome homogeneous broadening of EDF, the generating methods of multi-wavelength fiber lasers operated at room temperature based on stimulated Brillouin–Raman scattering [6], four-wave-mixing [7], polarization hole burning [8] and nonlinear optical loop mirrors [9], etc., have been demonstrated. Moreover to enhance practicality, some novel comb filters are continuously adopted in MWEDFLs, such as multimode fiber Bragg gratings, in-fiber Mach–Zehnder interferometer and microfiber knot resonator [10–15]. However, the flatness (uniform amplitude) and stability (peaking power and central wavelength) of the generated oscillations are not ideal in MWEDFLs due to the effects of mode-competition and self-pulse.

On one hand, to improve the flatness, nonlinear polarization rotation (NPR) is frequently used in the ring/linear-cavity-based MWEDFLs [16–22]. A typical NPR is generally formed by polarization controllers (PCs), polarizer and a section of single-mode fiber (SMF). Under the enough power of pump, NPR can efficiently constrain the mode-competition and equalize the intensity among different oscillations through inducing a suitable wavelength- and intensity-dependent loss. In general, the number of oscillations is positive, but the flatness is negative proportional to the pump power [17]. By finely adjusting PCs, the intensity difference of oscillations can be limited less than 1.4 dB [18]. On the other hand, to provide the stable outputs, Feng optimizes the operated parameters of optical

passive devices (e.g., the length of polarization-maintenance fiber (PMF) and SMF) [19]. Quan focuses on adjusting and optimizing the power of pumps [20]. Alimi and Han respectively introduce an optical feedback loop and PMF-based loop mirror into the NPR-based MWEDFLs [21,22]. According to the results in above articles, in a short period (~60 min), the power stability of MWEDFLs is maintained within 0.7~2.0 dB and the wavelength shift is generally less than 0.08 nm. Nevertheless, it is worth noting that the fluctuation of pump power and accumulation gain of EDF will be obvious with the increase of operation time, and they surely impact the working stability of MWEDFLs [22–25].

To enhance practicality, we propose a novel dual-ring-configuration-based scheme to simultaneously keep high flatness and stability within a long working term through hybrid optical-electrical control. In optical ring, a NPR-based ring cavity is formed by a C-band (1520~1560 nm) broadband source and a Lyot filter, and the high output power and flatness are obtained by optimizing the ratio of coupler and pump power. In electrical ring, a dual-channel fuzzy-controller with flexibility and robustness is introduced to simultaneously stabilize the power shift and wavelength shift of outputs by accurately adjusting the power of pump. The experiment results show that, our scheme achieves more than 10 stable oscillations in a MWEDFL with the dramatic improvements in flatness and working stability. Under dual-ring configuration, the output intensity of MWEDFL reaches ~−7.5 dBm with the flatness of ± 0.42 dB. And the in-stabilities in terms of power and central wavelength are respectively constrained ± 0.182 dBm and ± 0.029 nm within 10-h working period.

2. Principles and Setups

From Figure 1, the proposed MWEDFL is mainly composed of a broadband source (BBS), a comb filter (i.e., Lyot filter) and an electrical monitoring and controlling system. In such hybrid dual-ring configuration, BBS and Lyot filter form an optical ring cavity (denoted by Ring-1) to generate and flatten multi-wavelength oscillations in the band of 1550 nm through connecting a section of SMF, coupler (C1) and isolator. And the monitor and controller form an electrical negative-feedback ring (denoted by Ring-2) to further stabilize the outputs of MWEDFL.

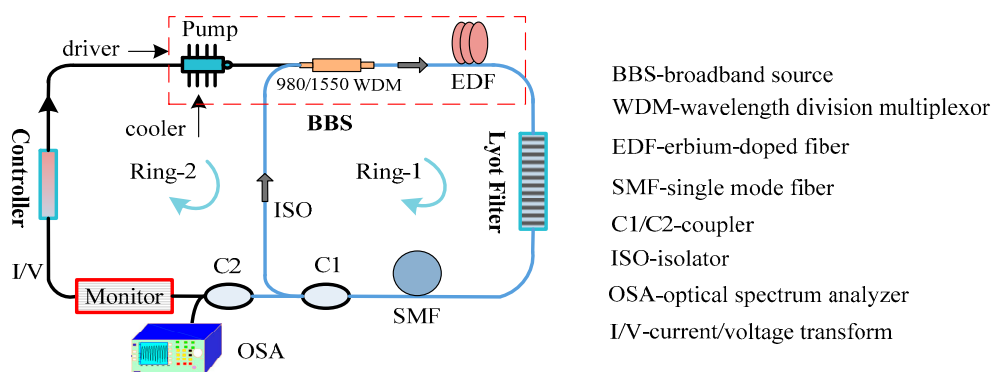


Figure 1. Scheme of multi-wavelength erbium-doped fiber laser (MWEDFL) with dual-ring configuration.

2.1. Optical NPR-Based Control for Flattening

In Ring-1, the BBS consists of a forward pump source (@974.9 nm, Oclaro, San Jose, CA, USA), a 980/1550 wavelength division multiplexor and a section of EDF (EDFC-980-HP-C, Nufern, East Granby, CT, USA) with fixed length. By a stable driver (LDC250C, Thorlabs, Newton, NJ, USA) and cooler (TED200C, Thorlabs, Newton, NJ, USA), the pump source can output the stable power of 0~330 mW, and the corresponding output of BBS is about 0~100 mW. As shown in Figure 2a, the Lyot filter is made up two PCs, an isolator, a polarizer and a section of PMF (PM1017C, YOFC, Wuhan, China). According to [19], the NPR effect will be generated in the combination of PC-SMF-PC-Polarizer and its transmission (T) can be depicted as

$$|T|^2 = \sin^2 \alpha_1 \sin^2 \alpha_2 + \cos^2 \alpha_1 \cos^2 \alpha_2 + \frac{1}{2} \sin(2\alpha_1) \sin(2\alpha_2) \cos(\Delta\varphi) \quad (1)$$

where α_1 and α_2 are respectively the incidence angle and emergence angle between the input light and SMF, and $\Delta\varphi$ denotes the summary of phase difference induced by PC ($\Delta\varphi_{PC}$), PMF ($\Delta\varphi_{PMF}$) and SMF ($\Delta\varphi_{SMF}$). Further, $\Delta\varphi_{PMF} = 2\pi L_p \cdot \Delta n / \lambda$ (where L_p is the length of PMF, Δn the refractive index difference), and $\Delta\varphi_{SMF} = -2\gamma L_s P \cdot \cos 2\alpha_1 / 3$, where γ and L_s is the nonlinear factor and length of SMF, P is the pump power. We then set $P = 100$ mW, $\lambda = 1550$ nm, $\Delta n = 0.00057$, $\gamma = 3W^{-1}km^{-1}$, $L_p = 10$ m, $\alpha_1 = \pi/3$, $\alpha_2 = 5\pi/6$, and the calculated transmission spectrum is shown as Figure 2b. The spectral-spacing is determined by $\Delta\lambda = \lambda^2 / \Delta n L_p$ and its value is ~ 0.44 nm. Moreover, a section of SMF (SMF-28e, Corning, Corning, NY, USA) with the length of 3.3 km is added to further enhance the non-uniformity of optical ring cavity.

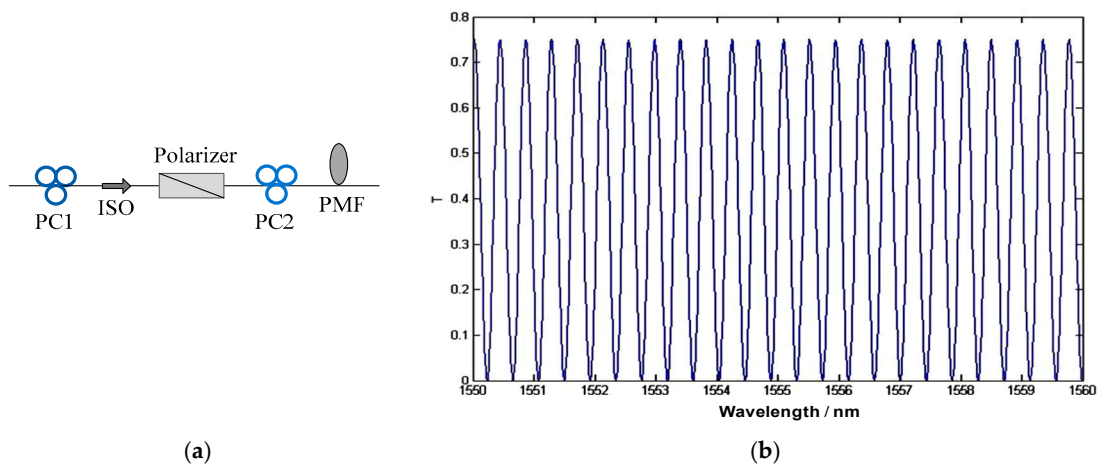


Figure 2. (a) The formed Lyot filter and (b) its calculated transmission spectrum (PC1/PC2: polarization controller, PMF: polarization-maintenance fiber, T: normalized transmission).

Under the enough pump power, the Lyot filter can be viewed as a saturable absorber and bring the inhomogeneous wavelength- and intensity-loss to alleviate the mode competition of oscillations caused by the homogeneous gain broadening of EDF. Consequently, the intensity among the oscillations is automatically balanced, and the flat outputs of MWEDFL will be observed by an optical spectrum analyzer (81642B, Agilent, Santa Clara, CA, USA) or a power meter (1830c, Newport, Irvine, CA, USA).

2.2. Electrical Control for Working Stability

In order to reduce the impacts from the fluctuation of pump power and accumulation gain of EDF, a dual-channel fuzzy-control scheme is adopted to stabilize the outputs of MWEDFL in a long and short working term. As shown in Figure 3, the input light from the coupler C2 enters the monitor. There are two channels in the designed monitor to respectively test the shifts of mean power and central wavelength of oscillations. A tunable Fabry-Perot filter (1554A, NewFocus, Newport, Irvine, CA, USA) is used in the wavelength-channel to lock the selective oscillation. The intensity changes of oscillations (denoted by λ -shift and P -shift, respectively) will be monitored by detector D1 and D2 (PDB450A, Thorlabs). After current-voltage (I/V) transform and amplifying, the sampled signals enter the differential amplifier *diff-1* and *diff-2*, and the corresponding errors e_λ and e_P will be gained through a subtraction operation with the set aim voltages (denoted by aim-1 and aim-2, respectively).

Fuzzy rule base is the essence of the designed one-level controller and it will deliver the factors (denoted by ε_λ and ε_P , respectively) to negatively feedback the shifts in terms of wavelength and mean peaking power, according to the values of e_λ and e_P . Set the membership of e_λ and e_P belonging to the subset: {High, MH (middle-high), N (normal), ML (middle-low), Low}, and the membership of

ε_λ and ε_P belonging to the subset: {PL (positive large), PM (positive middle), O (zero), NM (negative middle), NL (negative large)}. Concretely, the circuit of controller is shown in Figure 3, which is mainly composed of microcontroller unit (MCU), gain turning buttons and display. MCU (STM32F103C8T6) is the core of circuit and it conducts the digital subtraction operation, fuzzy control and outputs the feedback current. The output current can be displayed and amplified by the gain turning buttons in the range of $1\sim 10^3$. Moreover, we fabricate a new line with D-type 9-pin connector and input the current from driver into the circuit of controller. Finally, through a high precision amplifier (AD620), the feedback current and driving current are added and outputted.

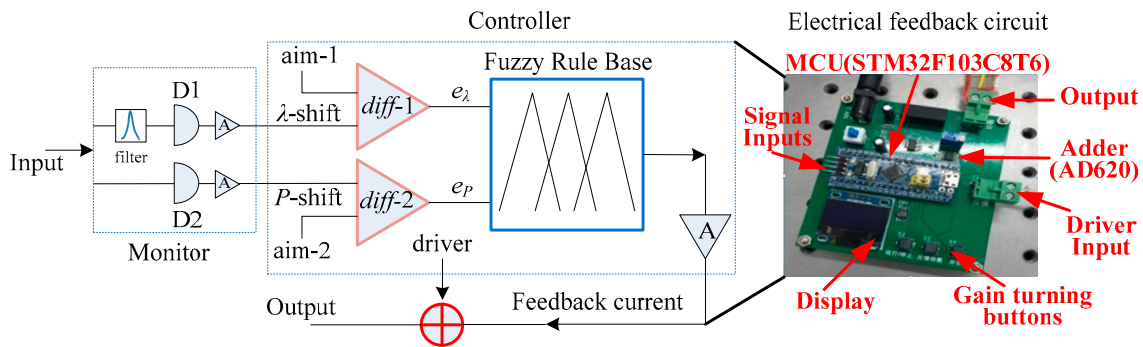


Figure 3. Scheme of dual-channel fuzzy controller, D1/D2: detector, A: amplifier, *diff-1/diff-2*: differential amplifiers, MCU: microcontroller unit.

Further, assuming the current of driver is I_d , the feedback currents (I_c) for λ -shift and P -shift are then presented as

$$I_\lambda = -a_1 \varepsilon_\lambda \cdot I_0 \tag{2}$$

$$I_P = -a_2 \varepsilon_P \cdot I_0 \tag{3}$$

where a_1 and a_2 are the gain factors, I_0 is the minimum of feedback current, accordingly $I_c = I_\lambda + I_P$. And through an adder, the output current I_{dc} will be

$$I_{dc} = I_d + I_c = I_d - (a_1 \varepsilon_\lambda + a_2 \varepsilon_P) I_0 \tag{4}$$

So, in the electrical Ring-2, I_{dc} is the final driving current for pump source and its value will be dynamically adjusted to enhance the working stability of MWEDFL. It is noted that the fuzzy rule base should be determined by the detailed e_λ and e_P , and it will be depicted in Section 3.

3. Experiments and Results

We set the length of EDF is 11 m, $L_{PMF} = 9.8$ m, $L_{SMF} = \sim 3.3$ km, the ratio of C2 (denoted by R_2) is 10/90, and the pump source operates in the range of 0~180 mW. Specially, the ratios of C1 (denoted by R_1) are 10/90, 20/80 and 50/50, respectively. We then set up a MWEDFL according to Figure 1 and conduct the comprehensive tests with respects to flatness and stability. Besides, the total connecting loss is smaller than 1.5 dB, and the room temperature is kept at 26 Celsius in experiments.

3.1. Optimization of Parameters and Flatness through Optical Ring Cavity

First of all, by varying pump power and R_1 , the outputs of MWEDFL are given in Figure 4 without electrical feedback. From Figure 4a, the mean output power is linearly increased with the raise of pump power, and when $R_1 = 50/50$ the maximum always occurs in the pumping range of 0~180 mW, obviously. Additionally, according to the results in Figure 4b–d, the smallest intensity difference (~ 2.87 dB) also occurs when $R_1 = 50/50$. Comparatively, the similar but larger intensity

differences (>4 dB) are presented when $R_1 = 10/90, 20/80$. In result the optimal output power and spectral flatness are obtained when $R_1 = 50/50$, although the number of oscillations is smaller.

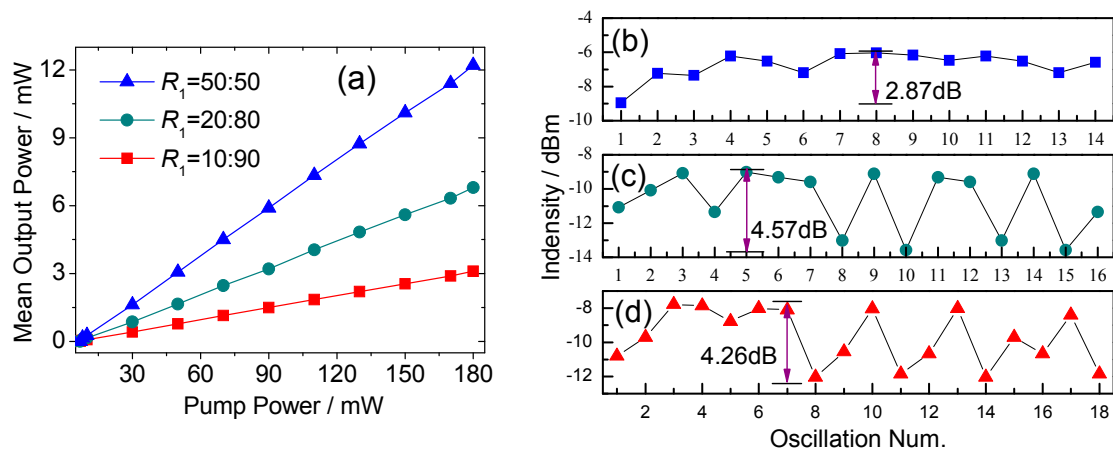


Figure 4. The outputs of MWEDFL with different ratios of C1, (a) mean output power by varying pump power, and the intensity of each oscillation at $P = 180$ mW when (b) $R_1 = 50/50$, (c) $R_1 = 20/80$, (d) $R_1 = 10/90$.

Under the condition of $R_1 = 50/50$, the output characteristics of MWEDFL are tested by varying pump power. From Figure 5a, the oscillation number is quickly increased in the range of $P = 0\sim70$ mW, but it is slowly and nonlinearly raised when $P > 90$ mW. Figure 5b shows the similar results also occur in term of mean intensity. Moreover, the stimulated green light with the central wavelength of 546 nm (may due to the excited state absorption in EDF [26]) is found and linearly increased with the addition of pump power (see Figure 5b). We then select $P = 113$ mW to get a trade-off among the oscillation number (>10), intensity (~ -7.5 dBm) and power of green light (<0.05 mW). Furthermore, the output spectrum of MWEDFL is flattened through accurately adjusting PCs position and pump power. As shown in Figure 6a, in the range of 1556.2~1560.7 nm there are 11 stable oscillations generated with an interval of 0.434 nm and the intensity difference reaches ± 1.54 dB within 3-dB bandwidth. Comparatively, we gain the ± 0.42 -dB flatness through a fine adjustment and the improvement of flatness is 72.7% ($= \frac{|\pm 0.42 - \pm 1.54|}{|\pm 1.54|}$) by calculation. Additionally from Figure 6b the side mode suppression ratio reaches over 30 dB.

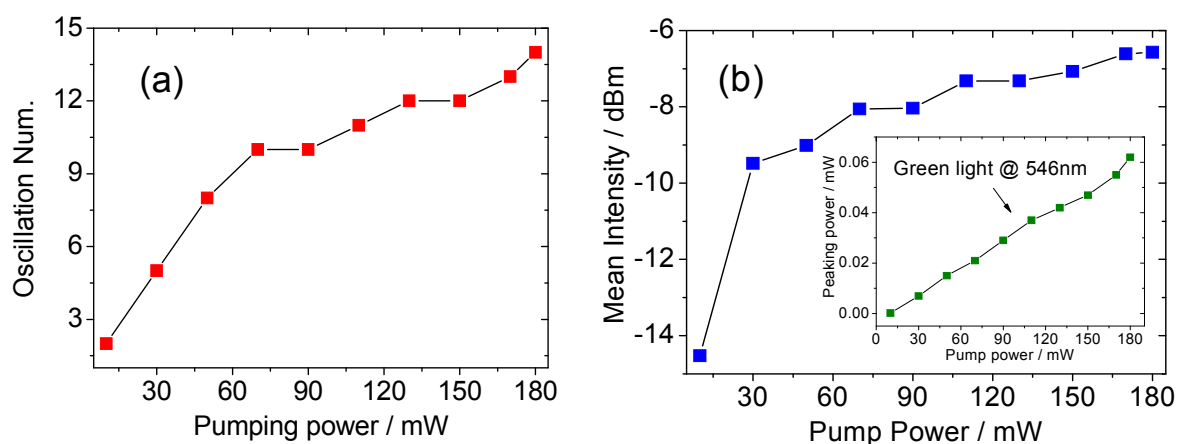


Figure 5. The outputs with varying pumping power when $R_1 = 50/50$, (a) oscillation number within 3-dB bandwidth; (b) mean intensity of oscillations (where the subfigure is stimulated green light with central wavelength of 546 nm).

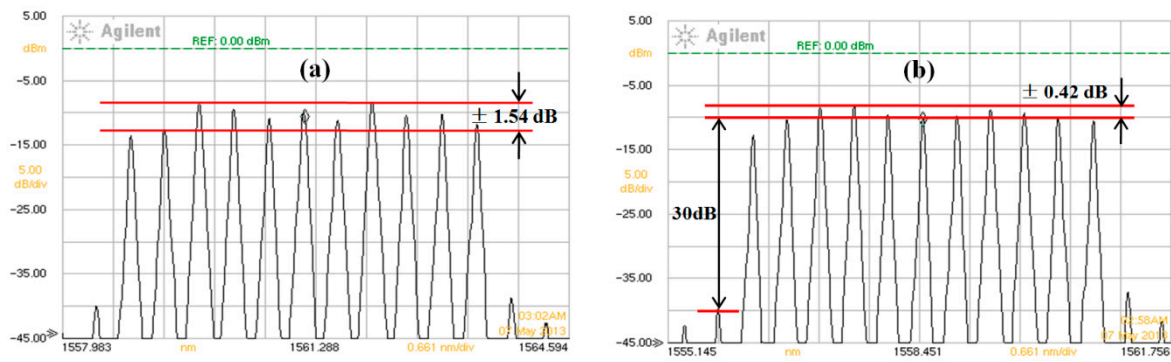


Figure 6. The output spectrum of oscillations at $P = 113$ mW and $R_1 = 50/50$, (a) coarse adjustment; (b) fine adjustment.

3.2. Improvement of Working Stability by Electrical Feedback Control

In this section, we set $P = 113$ mW, $R_1 = 50/50$, $R_2 = 10/90$, and $I_c = 0$, the working stabilities of MWEDFL are then tested in long and short terms, respectively. We find an obvious blue-shift occurs in the observed oscillation (@1560.46 nm) within a continuous 10-h (i.e., 600 min) operation. From Figure 7a, the total λ -shift is about ± 0.1 nm. And in Figure 7b the λ -shift in the short working term (50 min) is less than ± 0.07 nm. It means that the λ -shift of oscillations is small and stable in our designed MWEDFL. We define the change of λ -shift (denoted by $\Delta\lambda$) is

$$\Delta\lambda = \frac{e_\lambda}{e_{\lambda 0}} \tag{5}$$

where $e_{\lambda 0}$ is the base line of λ -shift. We according to the results in Figure 7a,b set $e_{\lambda 0} = 0.08$ nm, and the corresponding fuzzy subset of $\Delta\lambda$ is {MH (middle high), N (normal), ML (middle low)}. Its membership is shown as Figure 7c. Similarly, the changes of mean power in long and short working terms are presented in Figure 8a,b. The results show that the power fluctuation is over 1.0 dB but uniform within 10-h operation. Comparatively, there are some unexpected raises during the short-term testing and the total power shift also reaches ~ 1.0 dB. This indicates the P -shift of oscillations should be much concerned in MWEDFLs.

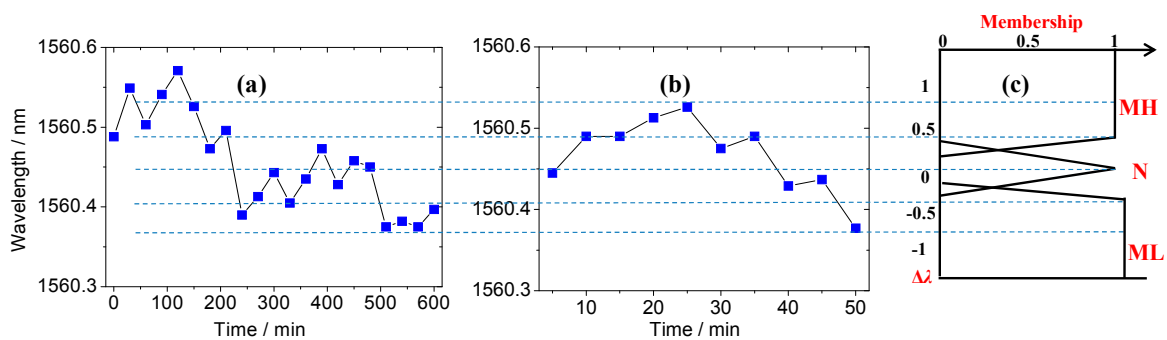


Figure 7. The wavelength shift of oscillation at 1560.46 nm in the (a) long term (600 min); (b) short term (50 min) and (c) the membership of λ -shift.

We define the change of P -shift (denoted by ΔP) is

$$\Delta P = \frac{e_P}{e_{P0}} \tag{6}$$

where e_{P0} is the base line of P -shift. Further we set $e_{P0} = 0.6$ dB according to the results in Figure 8a,b, and the corresponding fuzzy subset of ΔP is {H (high), MH (middle high), N (normal), ML (middle low), L (low)}. Its membership is shown as Figure 8c. Furthermore, we respectively set the fuzzy subsets of ϵ_λ and ϵ_P are {PM, O, NM} and {PL, PM, O, NM, NL}, and their corresponding memberships are shown in Figure 9. Consequently, the fuzzy rule bases for λ -shift and P -shift are given in Tables 1 and 2.

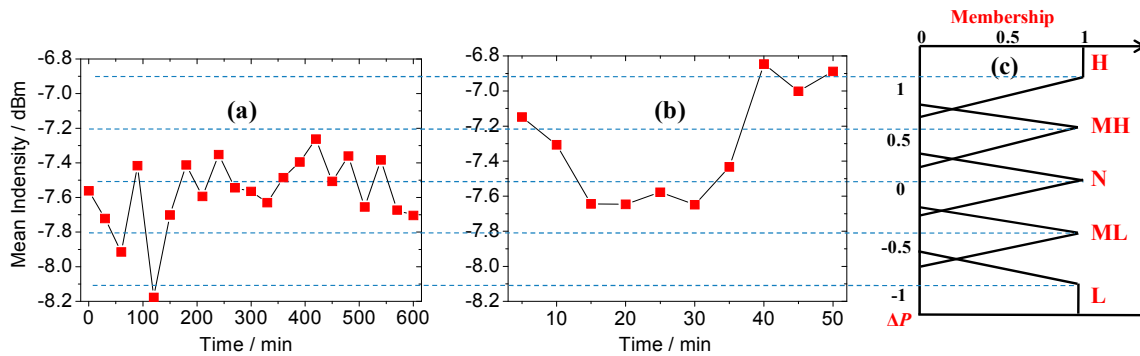


Figure 8. The mean intensity fluctuation of oscillations in the (a) long term (600 min); (b) short term (50 min) and (c) the membership of P -shift.

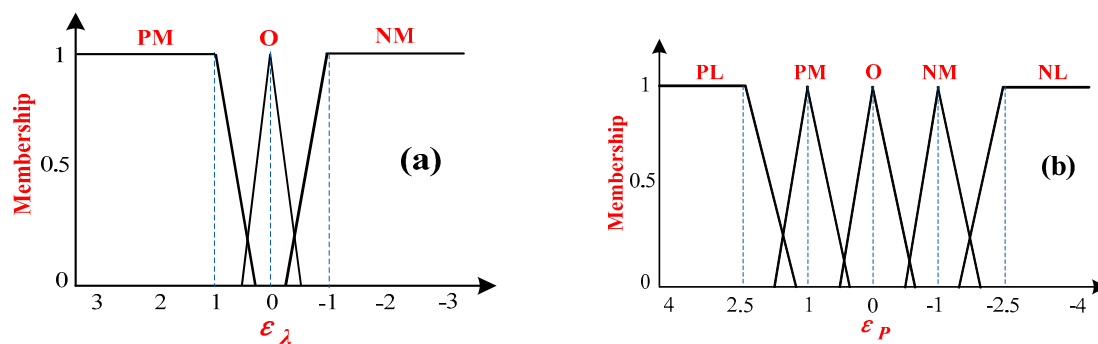


Figure 9. Factors of fuzzy control for (a) λ -shift and (b) P -shift.

Table 1. Fuzzy Rule base of λ -shift.

$\Delta\lambda$	ϵ_λ
MH	NM
N	O
ML	PM

Table 2. Fuzzy Rule base of P -shift.

ΔP	ϵ_P
H	NL
MH	NM
N	O
ML	PM
L	PL

We then set $a_1 = a_2 = 6.9 \times 10^2$ and $I_0 = 0.003$ mA, so in the controller the value of I_λ is in the range of $0 \sim \pm 2.07$ mA, and I_P is in the range of $0 \sim \pm 5.18$ mA. Under the electrical feedback controlling, the working stabilities of MWEDFL are demonstrated in Figure 10. Obviously, the blue-shift of central wavelength is efficiently constrained. From Figure 10a,b, the long-term (10-h) and short-term (50-min)

stabilities of wavelength shift are respectively ± 0.029 nm and ± 0.022 nm in our scheme. Furthermore, compared to the results in Figure 8, the power stability is dramatically improved by electrical controller. In Figure 10c,d, the power-shift is limited ± 0.182 dBm within 10-h period and the short-term shift of power reaches ± 0.141 dBm. By calculation the improvements of stability in terms of wavelength-shift and power-shift respectively reach 64.2% ($= (1 - \frac{0.029}{e_{\lambda 0}}) \times 100\%$) and 69.7% ($= (1 - \frac{0.182}{e_{p0}}) \times 100\%$) in our dual-ring configuration.

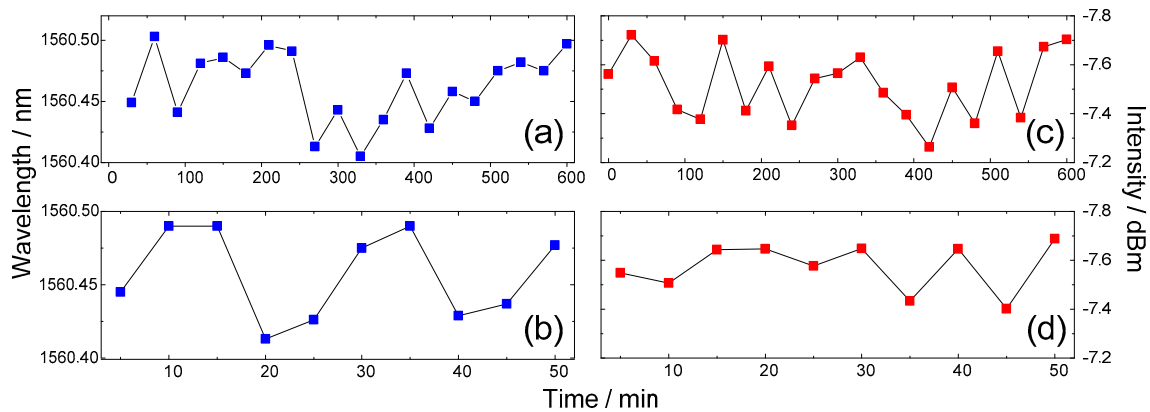


Figure 10. Wavelength shifts in (a) long term; (b) short term, and mean power fluctuations in (c) long term; (d) short term under electrical feedback controlling.

4. Conclusions

In a NPR-based ring-cavity MWEDFL, an electrical feedback control is introduced to improve the long- and short-term stability with respects to power and central wavelength. Under the optimal pump power and coupling ratio, we alleviate the stimulated green light and gain a -7.5 dBm mean intensity of oscillations with the flatness of ± 0.42 dB. Through an electrical fuzzy-control-based feedback, the wavelength shift of MWEDFL is constrained in 0.03 nm and its power shift is less than 0.2 dBm within 10-h continuous operation. With this hybrid automatic control, the improvements of stability in central wavelength and power are 64.2% and 69.7%, respectively. This is a very promising technology for practicality of multi-wavelength optical fiber laser.

Acknowledgments: This work is supported by National Natural Science Foundations of China (61675066, 61302075) and Youth Academic Backbone of Project of Heilongjiang University.

Author Contributions: Jiuru Yang conceived and designed the experiments; Xudong Zhang and Tiejing Li performed the experiments; Jiuru Yang analyzed the data; Jiuru Yang and Xudong Zhang wrote the paper.

Conflicts of Interest: The authors declare no conflict of interest.

References

1. Bellemare, A.; Karásek, M.; Rochette, M.; LaRochelle, S.; Têtu, M. Room temperature multifrequency erbium-doped fiber lasers anchored on the ITU frequency grid. *J. Lightw. Technol.* **2000**, *18*, 825–830. [[CrossRef](#)]
2. Zhan, L.; Ji, J.H.; Xia, J.; Luo, S.Y.; Xia, X.Y. 160-line multiwavelength generation of linear-cavity self-seeded Brillouin-erbium fiber laser. *Opt. Express* **2006**, *14*, 10233–10238. [[CrossRef](#)] [[PubMed](#)]
3. Iezzi, V.L.; Büttner, T.F.S.; Tehranchi, A.; Loranger, S.; Kabakova, I.V.; Eggleton, B.J.; Kashyap, R. Temporal characterization of a multi-wavelength Brillouin-erbium fiber laser. *New J. Phys.* **2016**, *18*. [[CrossRef](#)]
4. Diaz, S.; Lopez-Amo, M. Multiwavelength operation of erbium-doped fiber-ring laser for temperature measurements. *Opt. Laser Technol.* **2016**, *78*, 134–138. [[CrossRef](#)]
5. Chow, J.; Town, G.; Eggleton, B.; Ibsen, M.; Sugden, K.; Bennion, I. Multiwavelength generation in an erbium-fiber laser using in-fiber comb filters. *IEEE Photonics Technol. Lett.* **1996**, *8*, 60–62. [[CrossRef](#)]

6. Wang, Z.; Wanga, T.; Ma, W.; Jia, Q.; Su, Q.; Zhang, P. Tunable multiwavelength Brillouin-Raman fiber laser in a linear cavity with spectrum reshaped by Rayleigh scattering. *Opt. Fiber Technol.* **2017**, *36*, 327–333. [[CrossRef](#)]
7. Shirazi, M.R.; Taib, J.M.; Dimiyati, K.; Ahmad, H.; Harun, S.W. Multi-wavelength Brillouin-Raman fiber laser generation assisted by multiple four-wave mixing processes in a ring cavity. *Laser Phys.* **2013**, *23*. [[CrossRef](#)]
8. Cheng, J.; Chen, W.; Chen, G. Switchable quadruple-wavelength Erbium-doped fiber laser based on a chirped fiber grating and polarization-maintaining fiber. *Opt. Laser Technol.* **2016**, *78*, 71–73. [[CrossRef](#)]
9. Tian, J.; Yao, Y.; Xiao, J.; Xu, X.; Chen, D. Multiwavelength erbium-doped fiber laser based on intensity-dependent transmission in a linear cavity. *J. Appl. Phys.* **2011**, *109*. [[CrossRef](#)]
10. Feng, X.; Tam, H.; Chung, W.; Wai, P. Multiwavelength fiber lasers based on multimode fiber Bragg gratings using offset launch technique. *Opt. Commun.* **2006**, *263*, 295–299. [[CrossRef](#)]
11. Yan, J.; Fu, H.; He, S. Reconfigurable multiwavelength erbium-doped fiber laser using two multimode fiber Bragg gratings. *Microw. Opt. Technol. Lett.* **2010**, *49*, 1509–1511. [[CrossRef](#)]
12. Martinez-Rios, A.; Anzueto-Sanchez, G.; Monzon-Hernandez, D.; Salceda-Delgado, G.; Castellon-Uribe, J. Multiwavelength switching of an EDFL by using a fixed fiber-comb filter and a broad band tunable S-bent fiber filter. *Opt. Laser Technol.* **2014**, *58*, 197–201. [[CrossRef](#)]
13. Zou, H.; Yang, R.; Shen, X.; Wei, W. Stable and tunable self-seeded multiwavelength Brillouin-erbium fiber laser with higher OSNR. *Opt. Laser Technol.* **2016**, *81*, 180–183. [[CrossRef](#)]
14. Liu, M.; Liu, H.; Zheng, X.; Zhao, N.; Luo, A.; Luo, Z.; Xu, W. Demonstration of multiwavelength erbium-doped fiber laser based on a microfiber knot resonator. *IEEE Photonics Technol. Lett.* **2014**, *26*, 1387–1390. [[CrossRef](#)]
15. Xu, Y.; Ren, L.; Ma, C.; Kong, X.; Ren, K.; Song, F. Stable and uniform multiwavelength erbium-doped fiber laser based on a microfiber knot resonator with a Sagnac loop reflector. *J. Opt.* **2017**, *4*, 1–5. [[CrossRef](#)]
16. Li, Y.; Lou, C.; Wu, J.; Wu, B.; Gao, Y. Novel method to simultaneously compress pulses and suppress supermode noise in actively mode-locked fiber ring laser. *IEEE Photonics Technol. Lett.* **1998**, *10*, 1250–1252.
17. Park, N.; Wysocki, P.F. 24-line multiwavelength operation of erbium-doped fiber-ring laser. *IEEE Photonics Technol. Lett.* **1996**, *8*, 1459–1461. [[CrossRef](#)]
18. Wang, W.; Meng, H.; Wu, X.; Wang, W.; Xiong, R.; Xue, H.; Tan, C.; Huang, X. A nonlinear polarization rotation-based linear cavity waveband switchable multi-wavelength fiber laser. *Laser Phys. Lett.* **2013**, *10*. [[CrossRef](#)]
19. Feng, X.; Tam, H.; Wai, P. Stable and uniform multiwavelength erbium-doped fiber laser using nonlinear polarization rotation. *Opt. Express* **2006**, *14*, 8205–8210. [[CrossRef](#)] [[PubMed](#)]
20. Quan, M.; Li, Y.; Tian, J.; Yao, Y. Multifunctional tunable multiwavelength erbium-doped fiber laser based on tunable comb filter and intensity-dependent loss modulation. *Opt. Commun.* **2015**, *340*, 63–68. [[CrossRef](#)]
21. Al-Alimi, A.W.; Cholan, N.A.; Yaacob, M.H.; Abas, A.F.; Alresheedi, M.T.; Mahdi, M.A. Wide bandwidth and flat multiwavelength Brillouin-erbium fiber laser. *Opt. Express* **2017**, *25*, 19382–19390. [[CrossRef](#)] [[PubMed](#)]
22. Han, B.; Lou, S.; Zou, H.; Su, W.; Liu, C.; Zhang, J. A stable and uniform-amplitude multi-wavelength erbium-doped fiber laser based on nonlinear polarization rotation and a polarization-maintaining fiber loop mirror. *Laser Phys.* **2014**, *24*. [[CrossRef](#)]
23. Yang, J.; Ye, H.; Liu, C. Stabilize the output power of superfluorescent source by using hybrid controller. *Chin. J. Lasers* **2010**, *37*, 1520–1524. [[CrossRef](#)]
24. Puttnam, B.J.; Awaji, Y.; Wada, N. Gain-transient accumulation across EDFA cascades in optical packet-switched networks. In Proceedings of the 15th OptoElectronics and Communications Conference (OECC), Sapporo, Japan, 5–9 July 2010; pp. 408–409.
25. Zheng, W.; Ruan, S.; Zhang, M.; Liu, W.; Zhang, Y.; Yang, X. Switchable multi-wavelength erbium-doped photonic crystal fiber laser based on nonlinear polarization rotation. *Opt. Laser Technol.* **2013**, *50*, 145–149. [[CrossRef](#)]
26. Whitley, T.J.; Millar, C.A.; Wyatt, R.; Brierley, M.C.; Szebesta, D. Upconversion pumped green lasing in erbium doped fluorozirconate fiber. *Electron. Lett.* **2002**, *27*, 1785–1786. [[CrossRef](#)]

